JVI Journals.ASM.org

N-Glycans on the Nipah Virus Attachment Glycoprotein Modulate Fusion and Viral Entry as They Protect against Antibody Neutralization

Scott B. Biering,[a,c] Andrew Huang,[c] Andy T. Vu,[c] Lindsey R. Robinson,[c] Birgit Bradel-Tretheway,[a] Eric Choi,[c] Benhur Lee,[c,d,e] and Hector C. Aguilar[a,b]

Paul G. Allen School for Global Animal Health[a] and Department of Veterinary Microbiology and Pathology,[b] Washington State University, Pullman, Washington, USA, and Department of Microbiology, Immunology, and Molecular Genetics,[c]Department of Pathology and Laboratory Medicine,[d] and AIDS Institute,[e] David Geffen School of Medicine at UCLA, Los Angeles, California, USA

Nipah virus (NiV) is the deadliest known paramyxovirus. Membrane fusion is essential for NiV entry into host cells and for the virus' pathological induction of cell-cell fusion (syncytia). The mechanism by which the attachment glycoprotein (G), upon binding to the cell receptors ephrinB2 or ephrinB3, triggers the fusion glycoprotein (F) to execute membrane fusion is largely unknown. N-glycans on paramyxovirus glycoproteins are generally required for proper protein conformational integrity, transport, and sometimes biological functions. We made conservative mutations (Asn to Gln) at the seven potential N-glycosylation sites in the NiV G ectodomain (G1 to G7) individually or in combination. Six of the seven N-glycosylation sites were found to be glycosylated. Moreover, pseudotyped virions carrying these N-glycan mutants had increased antibody neutralization sensitivities. Interestingly, our results revealed hyperfusogenic and hypofusogenic phenotypes for mutants that bound ephrinB2 at wild-type levels, and the mutant's cell-cell fusion phenotypes generally correlated to viral entry levels. In addition, when removing multiple N-glycans simultaneously, we observed synergistic or dominant-negative membrane fusion phenotypes. Interestingly, our data indicated that 4- to 6-fold increases in fusogenicity resulted from multiple mechanisms, including but not restricted to the increase of F triggering. Altogether, our results suggest that NiV-G N-glycans play a role in shielding virions against antibody neutralization, while modulating cell-cell fusion and viral entry via multiple mechanisms.

Nipah virus (NiV) and Hendra virus (HeV) (genus *Henipaviridae*) have the highest mortality rates in the *Paramyxoviridae* family, which includes important viruses such as measles virus (MeV), mumps virus, human parainfluenza virus (hPIV), respiratory syncytial virus (RSV), and Newcastle disease virus (NDV). The reported mortality rate for NiV in humans is 40 to 92%, averaging 75% in the latest outbreaks (21, 25, 26, 43). NiV and HeV cause vasculitis, pneumonia, and encephalitis, which lead to death in a broad host range (11). Henipaviruses are biosafety level 4 (BSL4) agents with bio- and agroterrorism potential via animal-to-human and human-to-human transmission (4, 21, 43). Thus, henipaviruses have been classified as priority pathogens in the NIAID research agenda. These characteristics of NiV and HeV underscore the need for research and treatment development against these perilous pathogens.

Paramyxovirus membrane fusion is essential to viral entry and cell-cell fusion (syncytium formation), a mechanism for cell-to-cell viral spread. In addition, for the henipaviruses, syncytium formation is a pathognomonic signature, with microvascular endothelial cell syncytia found in brain, lung, kidney, and heart tissues (47). Membrane fusion generally requires the coordinated actions of the viral attachment (HN/H/G) and fusion (F) glycoproteins. The cell receptors ephrinB2 (B2) or ephrinB3 (B3) bind the NiV attachment glycoprotein (G) and activate it to undergo a conformational change (2) that results in triggering a fusion cascade in the class I fusion protein F (recently reviewed in references 3 and 4). Structurally, the henipavirus G glycoprotein has a receptor-binding globular head domain that consists of a six-bladed beta sheet-propeller (7, 48) connected to its transmembrane anchor via a flexible stalk domain. F is a class I fusion protein with canonical features common to its class, such as a hydrophobic fusion peptide and heptad repeats that bind each other to form a six-helix bundle, executing membrane fusion (22, 49). Mechanistic studies of class I fusion proteins have allowed the development of antiviral therapeutics for other viral families (i.e., for HIV) (30, 32). However, for the paramyxoviruses, there is a gap in our understanding of how receptor binding activates G to in turn trigger F to undergo a conformational cascade that results in membrane fusion. The elucidation of this event will likely assist antiviral therapeutic development.

N-glycans on the paramyxovirus fusion and attachment glycoproteins, as well as on the envelope glycoproteins of other viral families, have been shown to play important roles in proper glycoprotein expression, transport to the cell surface, fusion, viral entry, and/or antibody neutralization. For example, N-glycans on the dengue virus glycoprotein facilitate viral entry via binding to the C-type DC-SIGN lectin (33). N-glycans on the human immunodeficiency virus (HIV), influenza virus, West Nile virus, and Ebola virus have been shown to affect membrane fusion and/or viral infectivity (36, 45). In addition, glycoprotein N-glycans have

Received 24 May 2012 **Accepted** 12 August 2012

Published ahead of print 22 August 2012

Address correspondence to Hector C. Aguilar, haguilar@vetmed.wsu.edu, or Benhur Lee, bleebhl@ucla.edu.

S.B.B., A.H., and A.T.V. contributed equally to this article.

doi:10.1128/JVI.01304-12

been shown capable of "shielding" virions against antibody neutralization for viruses of several families, for example, HIV and simian immunodeficiency virus (SIV) (10, 37, 45), equine infectious anemia virus (EIAV) (39), hepatitis B virus (HBV) (23), and influenza virus (42; reviewed in reference 37). Moreover, HIV, NDV, influenza virus, and other viruses have the capacity to actually add N-glycans to their glycoproteins to escape antibody neutralization (13, 16, 42).

For the paramyxoviral glycoproteins, for example, those of NDV and canine distemper virus, removal of N-glycans has been reported to be detrimental to the glycoprotein's cell surface expression (CSE), membrane fusion, and viral entry (28, 36, 40, 44). In contrast, we and others reported that removal of N-glycans from NiV-F and HeV-F individually, and sometimes in combination, is not detrimental to cell surface expression or membrane fusion and in some cases actually increases cell-cell fusion and viral entry levels (6, 9, 31). These data suggest that most N-glycans in the henipavirus F glycoproteins are not essential for proper protein expression, folding, or transport to the cell surface and might actually inhibit membrane fusion. In addition, we observed that the N-glycans in NiV-F shield NiV virions against antibody neutralization (6). Furthermore, we reported that a specific N-glycan in NiV-F (F3) inhibits cell-cell fusion (6) and interacts with galectin-1, further facilitating membrane fusion inhibition (14, 24).

Despite these interesting findings, although two recent studies reported the chemical composition of the NiV-G (8) and HeV-G (12) N-glycans, the functions of the N-glycans in the henipavirus G glycoproteins remain unknown. We analyzed the roles of the NiV-G N-glycans by mutating the seven potential N-glycosylation sites individually or in combination. We discovered that specific N-glycans in NiV-G have important and unique roles in modulating cell-cell fusion and viral entry, as well as in providing a protective shield to virions against anti-NiV-G neutralizing antibodies. Our results, combined with previous findings for the functions of the henipavirus F N-glycans (6, 9, 31), highlight the unique roles N-glycans play in henipavirus pathobiology.

MATERIALS AND METHODS

Expression plasmids. Codon-optimized NiV-G and NiV-F genes, tagged at their C termini with the HA or AU1 tag, respectively, were utilized. Their constructs were previously described (24). The hyperfusogenic NiV-F N-glycan mutant F3F5 was also previously described (6). All of the NiV-G N-glycan mutants analyzed were constructed by site-directed mutagenesis, and their entire genes were sequenced.

Cell culture. CHO (CHOpgsA745) and Vero cells were cultured in minimal essential medium alpha with 10% fetal bovine serum (FBS). PK13 and 293T cells were cultured in Dulbecco modified Eagle medium with 10% fetal bovine serum (FBS). We obtained 293T and CHOpgsA745 cells from the American Type Culture Collection and PK13 (porcine fibroblasts) cells from Irvin Chen at the University of California at Los Angeles. CHOpgsA745 cells stably expressing ephrinB2 (CHOB2) were previously described and were cultured in CHO medium supplemented with 1 mg of G418/ml (35).

Quantification of syncytia. NiV-F and wild-type or mutant NiV-G expression plasmids (1:1 ratio, 2 μg total) were transfected into 293T cells growing in six-well plates at 80% confluence. At 18 to 24 h posttransfection, the cells were fixed in 2% paraformaldehyde, and cell-cell fusion was quantified by counting the number of nuclei within syncytia per ×200 field (five fields were counted per well and per experiment). For increased accuracy, each field was counted by multiple individuals, and the numbers of nuclei within syncytia per field counted were then averaged. Syncytia were defined as four or more nuclei visualized within a common cell membrane (6, 24).

Flow cytometry quantification of levels of NiV-F and NiV-G cell surface expression, ephrinB2 binding, and MAb binding. The production of anti-NiV-F polyclonal antisera 834 (34) and the production of monoclonal antibodies (MAbs) from genetically immunized rabbits (2, 19) were as previously described. The protocol for production of antisera 1187 was similar to the protocol for production of antisera 834, except that pcDNA3.1(+) plasmids expressing NiV-M and NiV-G were used instead of NiV-M and NiV-F. The binding of anti-NiV-F antiserum 834 to surface NiV-F and the binding of the anti-NiV-G specific rabbit MAbs (MAb26, MAb45, or MAb213) or mouse anti-hemagglutinin (anti-HA) MAb or soluble ephinB2 fused to human Fc (B2-hFc; R&D Systems, Minneapolis, MN) to cell surface NiV-G were measured by flow cytometry on NiV-F/G-transfected cells. Primary antibodies were used at a 1:1,000 dilution, and B2-hFc was used at 10 nM. Bound antibody or B2-hFc was detected with phycoerythrin-conjugated goat anti-rabbit, anti-mouse, or anti-human antibodies (Caltag, Burlingame, CA). Background values were obtained by binding equal concentrations of antibodies or B2-hFc and secondary reagents to pcDNA3.1 (mock)-transfected 293T cells and were subtracted from the cognate binding to NiV-F/NiV-G-transfected 293T cells.

Detection of glycoprotein expression and viral incorporation by Western blot analysis. Codon-optimized NiV-F and/or NiV-G expression plasmids (at a 1:1 ratio when in combination) were transfected into 293T cells plated in six-well plates (2 μg of plasmid DNA total), as indicated. Cells or pseudotyped NiV/VSV-rLuc virions were lysed in immunoprecipitation (IP) buffer (50 mM Tris [pH 7.5], 150 mM NaCl, 1 mM EDTA, 1% NP-40, 0.25% sodium deoxycholate, and 1× protease inhibitors [Roche Applied Science, Indianapolis, IN]). In the case of PNGaseF treatment to remove N-glycans, cell lysates were treated with 1× denaturing buffer (New England BioLabs [NEB], Inc., Ipswich, MA) and incubated at 60°C for 10 min prior to PNGaseF treatment (NEB). Cell lysates or viral lysates were then subjected to SDS-PAGE, and NiV-G or NiV-F glycoproteins were subsequently detected by Western blotting with anti-HA or anti-AU1 antibodies (Caltag, Burlingame, CA) at 1:5,000 and 1:3,000 dilutions, respectively. As loading controls, an anti-β-tubulin antibody was used at a 1:1,000 dilution (Santa Cruz Biotech, Inc., Santa Cruz, CA). Fluorescent secondary antibodies (Li-Cor Biosciences, Lincoln, NE) were used at a dilution of 1:10,000, respectively, and detected with a Li-Cor Odyssey fluorimager.

Quantitation of viral entry, viral genome copies, and viral neutralization. The NiV-F and wild-type or mutant NiV-G were pseudotyped onto a reporter vesicular stomatitis virus (VSV). 293T cells were transfected with the respective NiV-F/NiV-G expression plasmids and subsequently infected with recombinant VSV expressing the Renilla Luc reporter gene (VSV-ΔG-rLuc) (6, 34, 35). Viral supernatants were collected 36 h postinfection, and NiV/VSV-rLuc pseudotyped virions were purified over a 20% sucrose cushion. Vero cells plated in 96-well were infected with the NiV/VSV-rLuc virions in infection buffer (phosphate-buffered saline [PBS] plus 1% FBS) for 2 h at 37°C over a 5-log viral dilution span (10^{-2} to 10^{-6}). After 2 h, Vero cell growth medium was added. At 18 to 24 h postinfection, cells were lysed, and luciferase activity was measured as relative light units (RLU) using a *Renilla* luciferase detection system (Promega, Madison, WI) in an Infinite M1000 microplate reader (Tecan Group, Ltd., Männedorf, Switzerland). Quantitation of viral genome copies for the various NiV/VSV-rLuc viral preps was performed exactly as previously described (6). The amounts of RLU were then plotted against genome copies per milliliter and regressed using GraphPad Prism software, version 5.0. For quantification of antibody neutralization, viral entry assays were performed in the presence of the indicated dilutions (spanning 10^{-2} to 10^{-7}) of the specified anti-NiV-G specific antisera.

Coimmunoprecipitation of NiV-F and NiV-G. NiV/VSV-rLuc virions containing wild-type NiV-F and wild-type or mutant NiV-G were

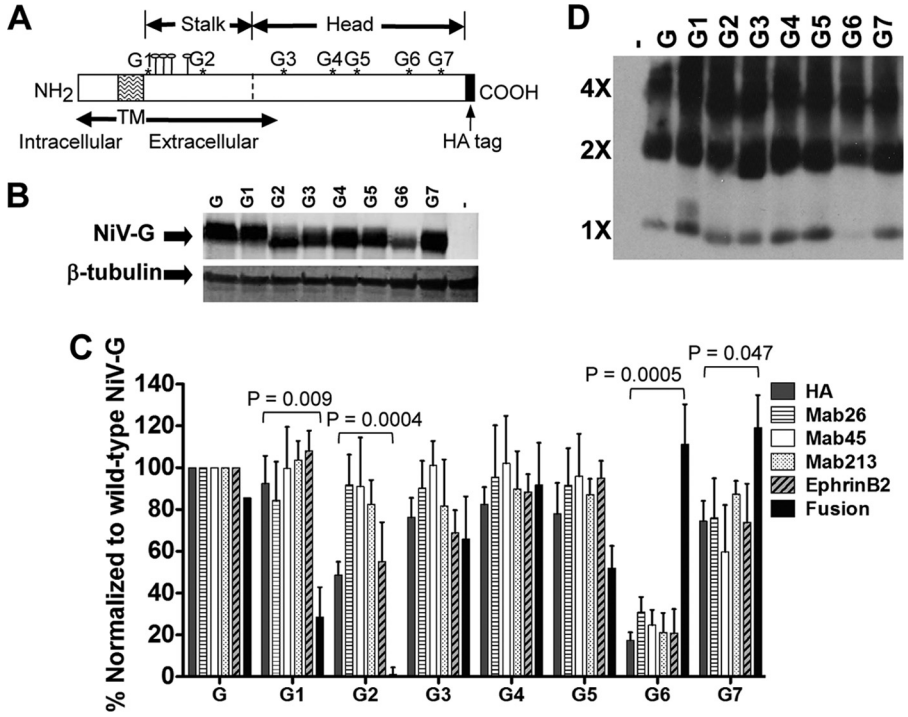

FIG 1 Analysis of NiV-G N-glycosylation site utilization and function. (A) Schematic of the NiV-G type II transmembrane glycoprotein with its intracellular N terminus and extracellular C terminus. Asterisks represent potential N-linked glycosylation sites G1 to G7. Mushroom-like structures between G1 and G2 in the stalk represent potential O-linked glycosylation sites. The extracellular C terminus is HA tagged. (B) Western blot analysis of wild-type and N-glycan mutant NiV-G from 293T cell lysates, showing their distinct relative gel mobilities. An anti-β-tubulin antibody was used as a cellular protein loading control. –, Vector control. (C) Relative levels of cell surface expression (HA), binding to MAbs (MAb26, MAb45, and MAb213), binding to soluble ephrinB2 receptor, and 293T cell-cell fusion. All levels for the mutants were separately normalized to levels seen for wild-type NiV-G, set at 100%. The data shown are averages plus standard deviations of four or more independent experiments. The *P* values shown were calculated with an unpaired Student *t* test and multiplied by 7, which takes into account the Bonferroni correction for multiple pairwise comparisons (wild-type NiV-G versus 7 mutants). (D) Western blot analysis of nonreduced NiV-G oligomers. 4×, 2×, and 1× denote tetramers, dimers, and monomers, respectively. –, Vector control.

lysed in IP buffer. Viral lysates were subjected to immunoprecipitation in IP buffer, essentially as previously described (6, 24), using magnetic protein G-beads conjugated to an anti-HA antibody (Miltenyi Biotech, Auburn, CA). Coimmunoprecipitated (co-IP) proteins were analyzed by Western blotting as described above using the appropriate anti-tag antibody and quantified using a Li-Cor Odyssey fluorimager.

F-triggering assay. F-triggering assays were performed essentially as previously described (1, 2). Briefly, CHO cells were transfected with F, G, and green fluorescent protein (GFP) expression plasmids, at a 13:6:1 ratio, respectively. At 18 h posttransfection, a 1:1 ratio of the transfected CHO cells and untransfected CHO (negative control), or CHOB2 cells, were mixed and incubated for 90 min at 4°C or 37°C in the presence of excess (1 μM) biotinylated heptad repeat 2 (HR2) peptide (biotin-KVDISSQISSM NQSLQQSKDYIKEAQRLLDTVNPSL). Subsequently, the cells were moved back to 4°C, washed with wash buffer (1% FBS in PBS), fixed in 2% paraformaldehyde for 15 min, and washed again twice with wash buffer. The biotinylated HR2 peptide bound to F was detected using allophycocyanin (APC)-conjugated streptavidin and quantified by flow cytometric analysis. To enhance our signals and signal/noise ratios, an APC amplification kit was used (Miltenyi Biotec, Auburn, CA), and we focused our analysis on F-expressing cells by gating on bright GFP-positive cells and analyzing for APC fluorescence within the GFP++ gate.

RESULTS

NiV-G is glycosylated at six of its seven potential N-linked glycosylation sites. There are seven potential N-linked glycosylation sites in NiV-G (Fig. 1A). To determine whether these sites are indeed glycosylated, we made conservative asparagine to glutamine (N to Q) mutations in position 1 of each N-glycosylation sequon $N^1X^2(S/T)^3$ (mutants G1 through G7 from the intracellular N- to the extracellular C terminus) (Fig. 1A). We then examined the expression and relative mobilities of the wild-type and mutant G glycoproteins from transiently transfected 293T cells by Western blot analysis. Our results revealed faster migration of all but one (G1) mutant glycoproteins relative to the wild-type G (Fig. 1B), indicating that except for the membrane-juxtaposed G1 site, all potential N-glycosylation sites were N glycosylated (G2 to G7). To be absolutely certain that the gel shifts were a result of differences in N glycosylation, we treated our cell lysates with PNGaseF. This treatment resulted in a reduction of the apparent molecular mass of approximately 10 to 12 kDa overall (corresponding to five to six N-glycans) and completely eliminated the gel shifts for all mutants G2 to G7 relative to wild-type G (data not shown).

In addition, it appeared that mutants G2 and G6 were expressed at lower levels than the wild-type G glycoprotein in whole-cell lysates (Fig. 1B). To determine whether the levels of whole-cell expression corresponded to expression levels at the cell surface, we measured the relative cell surface amounts of wild-type and mutant glycoproteins via flow cytometry using an MAb specific to the C-terminal extracellular HA tag (Fig. 1A). Our results showed that mutants G2 and G6 were indeed expressed at lower levels than those of wild-type NiV-G at the cell surface (ca. 50 and 20%,

respectively) (Fig. 1C). In addition, our flow cytometry analyses corroborated that all of the other NiV-G N-glycan mutants were expressed at the cell surface at levels roughly similar (or slightly lower) relative to those of the wild-type NiV-G glycoprotein.

In addition to estimate the effects of N-glycan removal on the gross conformational integrities of the mutant glycoproteins, we measured the binding abilities of a panel of conformational anti-NiV-G specific MAbs (MAb26, MAb45, and MAb213) (2, 19) to the wild-type or mutant glycoproteins by flow cytometry. (Importantly, we showed that this panel of anti-NiV-G MAbs are conformational, since they efficiently detect native [yield strong flow cytometry signals], but not denatured NiV-G [yield extremely weak to null Western blot signals] [2; data not shown].) We then normalized these MAb binding signals to that of the wild-type NiV-G arbitrarily set at 100% (Fig. 1C). We then compared the normalized MAb binding levels to those of the normalized anti-HA antibody binding signals (cell surface expression levels). Our results suggested that all NiV-G N-glycan mutant glycoproteins had overall conformations grossly similar to the wild-type NiV-G, as they displayed similar levels of binding to MAb26, MAb45, and MAb213 relative to their levels of cell surface expression (Fig. 1C). The only exception, mutant G2, displayed 70 to 85% enhancement of binding to MAb26, MAb45, and MAb213 over its cell surface expression levels (HA binding), suggesting that removal of the G2 N-glycan may have an effect in the overall NiV-G conformation. Alternatively, because all of the MAbs seem to have increased levels of binding to mutant G2, the anti-HA antibody binding to this mutant may be relatively lower than that of the wild-type G, or removal of the G2 N-glycan itself may allow for greater levels of binding of all three MAbs to mutant G2. We believe the former alternative is very unlikely because the HA tag is at the ectodomain C terminus; however, since we have not mapped the binding epitopes for the MAbs, the latter is a formal possibility.

NiV-G N-glycans modulate membrane fusion. To investigate whether N-glycans affect the ability of NiV-G to promote membrane fusion, we measured the abilities of the N-glycan mutants (G1-G7) to induce 293T cell-cell fusion (syncytia) (Fig. 1C). Since we and others have shown that the levels of cell-cell fusion the henipavirus glycoproteins promote depend on their cell surface expression (CSE) levels (6, 46), we calculated a fusion index as a ratio of normalized cell-cell fusion to normalized CSE (Table 1; see Fig. 1C for HA signals), as previously calculated for our NiV-F fusion mutants (5, 6). Thus, the fusion index for wild-type NiV-G would be: 100% fusion/100% CSE = 1, and fusion indexes above or below 1 would reflect hyper- or hypofusogenic phenotypes, respectively. Interestingly, we observed that the NiV-G stalk mutants G1 and G2 displayed hypofusogenic phenotypes, with G2 yielding very strong and G1 yielding mild hypofusogenic phenotypes (fusion indexes of 0.0 and 0.3, respectively, and P values, including Bonferroni corrections, of 0.009 and 0.004, respectively, Fig. 1C and Table 1). In contrast, although the level of cell surface expression for mutant G6 was very low (17% of wild-type G), its level of induction of cell-cell fusion was similar to that of wild-type G (111%), yielding a strong hyperfusogenic index of 6.4 and $P = 0.0005$. In comparison, mutant G7 displayed near-wild-type levels of CSE and a slight hyperfusogenic fusion index of 1.6, and $P = 0.047$ (Fig. 1C and Table 1). These results are interesting, since paramyxovirus attachment protein hyperfusogenic phenotypes are rare, and to our knowledge those previously reported for the paramyxoviruses always involved increases in receptor binding avidities (29), whereas our G6, G7, and other hyperfusogenic mutants discussed below did not (Fig. 1C).

TABLE 1 Fusion/CSE ratios for wild-type and N-glycan mutant NiV-G glycoproteins[a]

NiV-G Env	CSE	Fusion	Fusion index (fusion/CSE ratio)
G	100	100	1.0
G1	92	29	0.3
G2	49	1	0.0
G3	76	66	0.9
G4	82	92	1.1
G5	78	52	0.7
G6	17	111	6.4
G7	74	119	1.6
G2G3	25	2	0.1
G2G6	32	5	0.2
G3G6	48	43	0.9
G4G5	41	104	2.5
G4G7	101	417	4.1
G5G6	31	99	3.2
G5G7	62	126	2.0
G6G7	51	74	1.5
G2G3G6	16	6	0.4
G4G5G6	24	142	5.9
G4G6G7	18	122	6.7
G5G6G7	24	59	2.4

[a] The cell surface expression (CSE) and cell-cell fusion levels of the NiV-G N-glycan mutants were within the previously shown linear ranges of these assays (Aguilar et al. [6]). Both fusion (nuclei inside syncytia) and CSE (mean fluorescence intensity) levels were normalized to that of wild-type NiV-G, set at 100%. The ratios of the normalized fusion to CSE values were calculated for each mutant. By definition, the fusion/CSE ratio of the wild-type NiV-G would be 1.0 (100%/100%).

Another factor that can influence the ability of viral envelope glycoproteins to promote membrane fusion is their receptor binding avidity. Thus, we determined whether N-glycan removal affected the levels of binding of our hypo- and hyperfusogenic NiV-G N-glycan mutants to soluble ephrinB2 receptor (B2-hFc), relative to wild-type NiV-G, by flow cytometry. The receptor-binding levels for all mutants were roughly similar to each mutant's relative levels of cell surface expression, as determined by anti-HA antibody binding (Fig. 1C). These data indicate that the hypo- or hyperfusogenic phenotypes of the NiV-G N-glycan mutants were not due to aberrant levels of receptor binding. Therefore, we uncovered NiV-G N-glycan mutants that affect a post-receptor-binding step(s) in the fusion cascade.

In addition, since cysteine mutations in the NiV-G stalk domain have been shown to affect G oligomerization strength and consequently membrane fusion (27), we sought to determine whether removal of N-glycans altered the ability of NiV-G to homo-oligomerize into dimers and tetramers (Fig. 1D). This is particularly important for the G2 mutant, which is located in the NiV-G stalk domain. We subjected the lysates of 293T cells expressing the wild-type or mutant glycoproteins to nonreducing Western blot analysis. In contrast to the cysteine stalk mutants (27), we found that all N-glycan mutants were able to homo-oligomerize to form dimers and tetramers similarly to the wild-type NiV-G. These data indicate that no individual N-glycan is essential to achieving proper NiV-G homo-oligomerization. Furthermore, these results suggest that the hypo- and hyperfusogenic phenotypes observed for the NiV-G N-glycan mutants were not

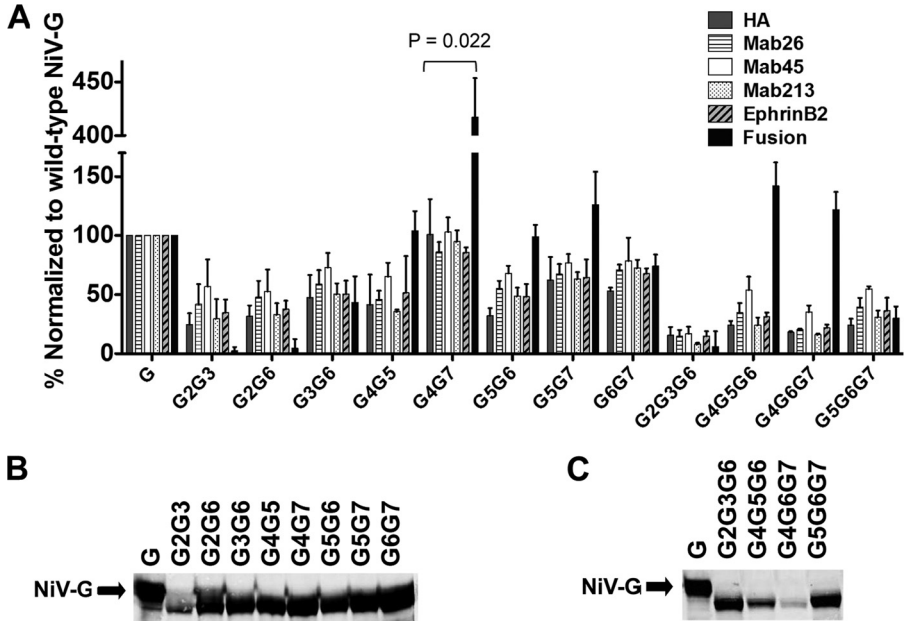

FIG 2 Synergistic and antagonistic effects of multiple NiV-G N-glycans in combination on cell-cell fusion. (A) Relative levels of 293T cell surface expression (HA), binding to MAbs (MAb26, MAb45, and MAb213), binding to soluble ephrinB2 receptor, and cell-cell fusion. All levels for the mutants were separately normalized to levels seen for wild-type NiV-G, set at 100%. The data shown are averages plus standard deviations of three or more independent experiments. The *P* value shown for mutant G4G7 was calculated with an unpaired Student *t* test and multiplied by 12, which takes into account the Bonferroni correction for multiple pairwise comparisons (wild-type NiV-G versus 12 mutants). The axis was broken to aid the visualization of the results for most mutants. (B) Western blot analysis of double N-glycan mutants in 293T cell lysates, displaying their gel mobility differences from the wild-type NiV-G. A representative image out of three independent experiments is shown. (C) Western blot analysis of triple N-glycan mutants in 293T cell lysates, displaying their gel mobility differences from the wild-type NiV-G. A representative image out of three experiments is shown.

due to aberrant levels of oligomerization. (Note that for mutant G6 less monomer was observed due to lower overall expression levels of this mutant, but the monomer band was clearly observed at higher exposure times [data not shown].)

Lastly, to corroborate that the cell-cell fusion levels we observed in 293T cells were not unique to this cell line, we repeated our cell-cell fusion assays in Vero cells. These cells yielded relative levels of cell-cell fusion for all mutants that were roughly similar to those of 293T cells (data not shown). Overall, our results indicate that removal of individual N-glycans from NiV-G results in altered cell-cell fusion levels and that these effects are not due to the mutant's aberrant levels of cell surface expression, receptor binding, or homo-oligomerization.

Effects of removal of multiple N-glycans on membrane fusion. To determine the potential synergistic or antagonistic (or dominant negative) effects of N-glycans on cell-cell fusion, we mutated two or three N-glycosylation sites (N to Q) simultaneously. We selected specific double or triple N-glycan mutations to be inclusive of all of the fusion phenotypes of the single N-glycan mutants in Fig. 1 and Table 1 (top). Analysis of the double or triple N-glycan mutants revealed that the G2 hypofusogenic phenotype was dominant over the hyperfusogenic or wild-type phenotypes. Mutants G2G3, G2G6, and G2G3G6 all yielded hypofusogenic fusion indexes of 0.1, 0.2, and 0.4, respectively (Fig. 2A and C and Table 1). Importantly, the fusion phenotypes of these mutants were not simply due to decreased levels of total cell expression (Fig. 2B), cell surface expression (anti-HA signals in Fig. 2A and Table 1), or ephrinB2 receptor binding (Fig. 2A).

In addition, we observed context-dependent synergistic or dominant-negative effects for the removal of multiple NiV-G N-glycans. As expected, many of the double and triple mutants that did not contain a mutation in the G2 site but contained mutations in the G6 and G7 sites yielded slight to strong hyperfusogenic phenotypes (mutants G4G7, G5G6, G5G7, G6G7, G4G5G6, G4G6G7, and G5G6G7, with fusion indexes of 4.1, 3.2, 2.0, 1.5, 5.9, 6.7, and 2.4, respectively, Fig. 2A and Table 1). Interestingly, however, mutant G4G7 yielded a significantly greater fusion index (4.1, and $P = 0.0018 \times 12$ [Bonferroni factor] $= 0.022$) than the individual mutation of the G4 or G7 sites (1.1 and 1.6, respectively), suggesting a synergistic effect of the simultaneous removal of the G4 and G7 N-glycans. Again, this phenotype is extremely rare, as previously reported paramyxovirus hyperfusogenic attachment protein mutants had increased receptor binding avidities (29), while our NiV G G4G7 mutant did not. On the other hand, mutation G6G7 yielded a fusion index lower than expected (1.5), since G6 and G7 yielded fusion indexes of 6.4 and 1.6, respectively, suggesting a dominance of the G7 phenotype over the G6 phenotype.

Overall, our data indicate that the effects of removing multiple N-glycans on the fusogenic capacities of NiV-G are highly context dependent. As further examples, the double N-glycan mutant G4G5 did not contain mutations in the hyperfusogenic sites G6 or G7 but yielded a hyperfusogenic phenotype (fusion index of 2.5) despite the fusion indexes of 1.1 and 0.7 for the individual G4 and G5 mutants, respectively. In addition, a double N-glycan mutant with a mutation in the hyperfusogenic G6 site was not hyperfusogenic (mutant G3G6 with a fusion index of 0.9). These phenotypes suggest that the mechanisms that give rise to the synergistic or

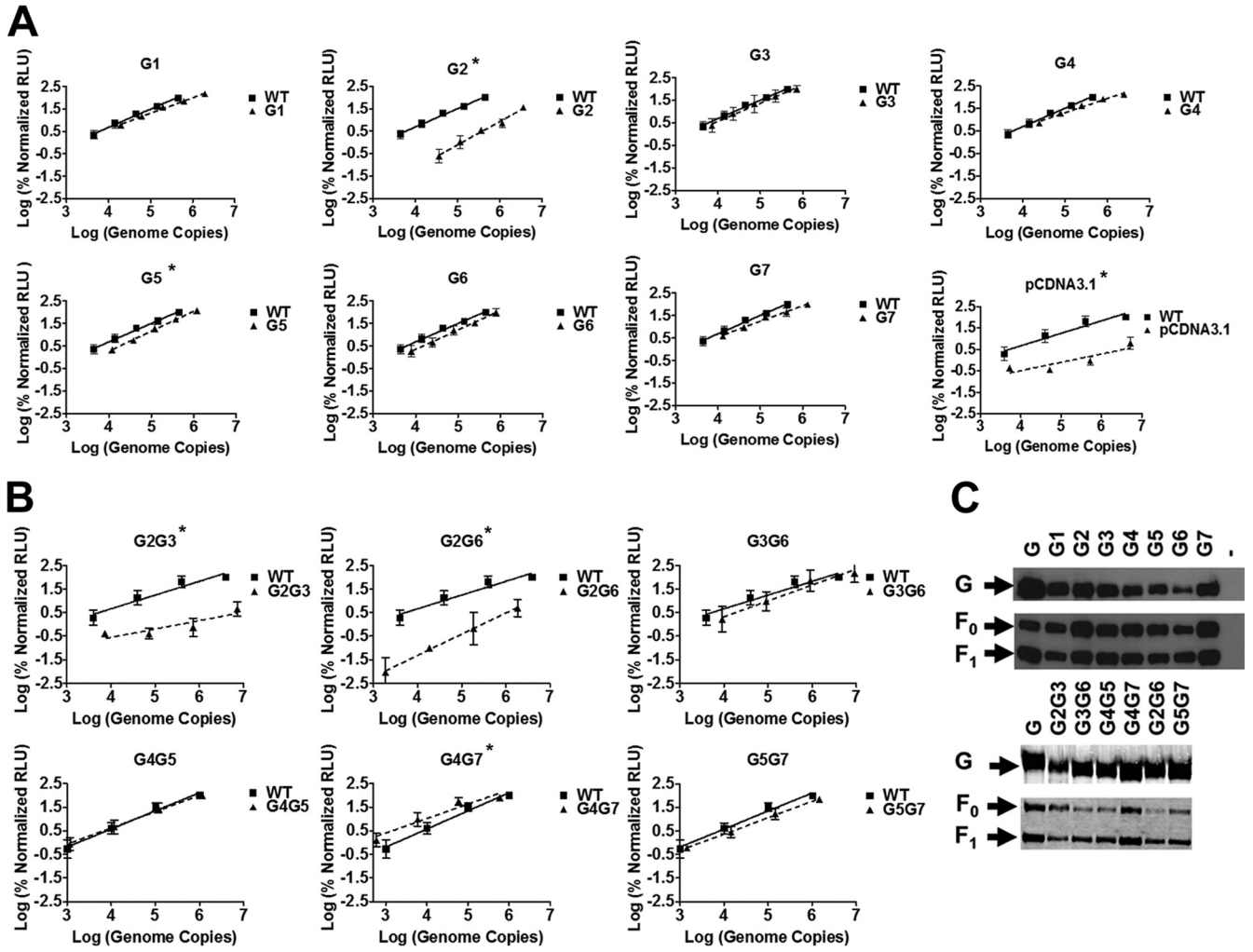

FIG 3 Effect of N-glycan removal on viral entry. (A and B) Relative entry levels of NiV-F/G-pseudotyped VSV-*Renilla* luciferase reporter viruses (VSV-rLuc). NiV-F and the indicated wild-type or individual (A) or double (B) N-glycan mutant NiV-G glycoproteins were pseudotyped onto luciferase reporter viruses as described in Materials and Methods. RLU were quantified 18 to 24 h postinfection and plotted against the number of viral genomes per ml. The relative amounts of genome copies in the viral preparations were analyzed by quantitative reverse transcription-PCR as described in Materials and Methods. The data shown are averages ± the standard deviations from three or more independent experiments. Sometimes the standard deviation bars are not visible because they are too small to be seen in a logarithmic scale. *, Mutants for which *P* values calculated using the Student *t* tests showed statistically significant differences ($P < 0.05$) between the wild-type and mutant levels of viral entry at several given genome copy numbers. (C) Western blot analysis of wild-type or mutant NiV-G glycoproteins contained in viral preparations used in panels A and B and blotted with a mouse anti-HA MAb, as described in Materials and Methods. One representative image out of three independent experiments is shown. –, Vector control.

dominant-negative fusion phenotypes produced by removal of N-glycans are highly context dependent and that the roles of the NiV-G N-glycans in membrane fusion may have some redundancy.

NiV-G N-glycans modulate viral entry. We then sought to determine whether the hyper- and hypofusogenic phenotypes displayed by the NiV-G N-glycan mutants in cell-cell fusion assays corresponded to increases or decreases in viral entry, respectively. To avoid the need of a reverse-genetics system at BSL-4 containment, we used our previously established BSL-2 viral entry assay. We pseudotyped wild-type NiV-F and wild-type or selected NiV-G N-glycan mutants onto vesicular stomatitis virions (VSV) that lacked their own glycoprotein (VSV-ΔG) but expressed the *Renilla* luciferase reporter gene (VSV-ΔG-rLuc) (5, 6). We constructed NiV/VSV-rLuc virions representative of all of the fusion phenotypes in Fig. 1 and 2. To accurately determine the viral entry efficiencies of our mutants, for each purified viral preparation we quantified the concentration of viral particles by measuring the number of VSV genome copies using quantitative reverse transcription-PCR (Fig. 3A and B). We then quantified the levels of infectivity of Vero cells by our pseudotyped virions over several orders of magnitude of viral input (genome copies per milliliter) (Fig. 3A and 3B). We also monitored the amount of wild-type and mutant NiV envelope glycoprotein incorporated into the pseudotyped virions by Western blot analysis (Fig. 3C).

In general, cell-cell fusion phenotypes (Fig. 1 and 2 and Table 1) correlated to the levels of entry of our single (Fig. 3A) and double (Fig. 3B) N-glycan mutant pseudotyped virions. For example, all virions that contained the G2 mutation (mutants G2, G2G3, and G2G6) were basically noninfectious compared to bald

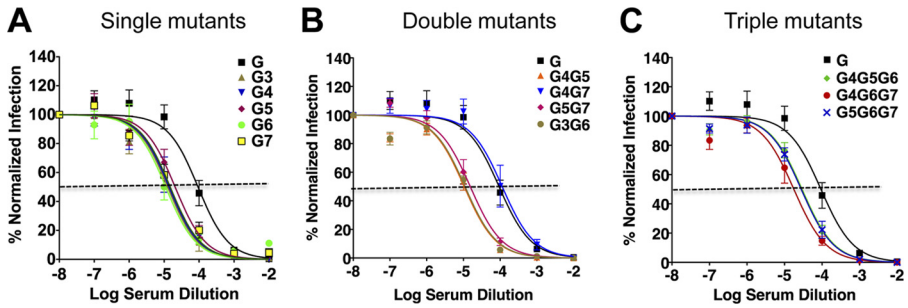

FIG 4 NiV-G N-glycans protect NiV against neutralizing antibodies. (A to C) Viral entry of pseudotyped NiV/VSV-rLuc virions that incorporated wild-type NiV-F and wild-type or mutant NiV-G. Viral entry levels were neutralized with various concentrations of anti-NiV-G specific polyclonal antiserum (i.e., antiserum 1187) and detected by measuring luciferase activity as relative light units (RLU) at 18 to 24 h postinfection. Single (A), double (B), and triple (C) N-glycan mutants were tested. Logarithms of the dilutions of 1-mg/ml serum stocks are shown. Averages ± the standard deviations of four independent experiments, with triplicate wells per experiment, are shown. All mutants except for G4G7 showed Student *t* test *P* values of <0.05 over a range of several log serum dilutions.

particles (sample pcDNA3.1). Mutant G4G7 virions were somewhat hyper-infective (note the log scale) (Fig. 3A and B), and mutant G5 was slightly hypoinfective. Furthermore, other mutants showed roughly similar levels of viral entry to the wild-type virions. Importantly, neither the hyperinfective phenotype of the G4G7-containing virions nor the hypoinfective phenotypes of the G2-containing virions were due to significant increases or decreases, respectively, in their relative levels of incorporation of the G N-glycan proteins into virions compared to those of wild-type G virions (Fig. 3C).

NiV G N-glycans protect virions from neutralizing antibodies. Removal of most N-glycans, with the exception of G2, resulted in near-wild-type or hyperfusogenic phenotypes (Fig. 2 and 3) as measured by cell-cell fusion and viral entry assays. Therefore, it appears that most N-glycans are dispensable (at least individually) for proper protein expression, folding, and transport to the cell surface. Then, what is the biological role of the NiV-G N-glycans? It has been proposed that N-glycans play a role as a "glycan shield" against neutralizing antibodies for other viral families (10, 37, 45). We also reported that the N-glycans in NiV-F shield NiV against neutralizing antibodies (6). Taking advantage of our ability to measure viral entry for most of our NiV/VSV-rLuc-pseudotyped NiV-G N-glycan mutant virions (with the exception of virions containing the G2 mutation), we sought to determine whether removal of NiV-G N-glycans played a role in antibody neutralization.

We observed that the removal of any of the single NiV-G N-glycans (G3 to G7) resulted in increased neutralization sensitivity to two distinct anti-NiV-G specific polyclonal antisera: 1187 (Fig. 4A) and 806 (data not shown). An ~10-fold difference (note the logarithmic scale) was observed between the antibody 1187 50% inhibitory concentration (IC_{50}) for the wild-type (an approximately 1:10,000 antibody dilution) versus the N-glycan mutant virions (an approximately 1:100,000 antibody dilution) (Fig. 4A). These data strongly suggest that, similarly to the NiV-F N-glycans (6), the NiV-G N-glycans play a role in protecting NiV against antibody neutralization.

We further sought to determine whether the removal of two or three N-glycans simultaneously would result in even greater levels of increased neutralization sensitivity. We observed basically no additional increases in neutralization sensitivity for any of the double N-glycan mutant virions tested compared to the single N-glycan mutant virions. Surprisingly, instead we observed reduced neutralization sensitivity for one double mutant, G4G7, for which the IC_{50} was similar to that of the wild-type virions (1:10,000 antibody dilution) (Fig. 4B). We reasoned that this phenotype might be due to relatively faster viral entry kinetics for this mutant in comparison to the wild-type virions. However, when we modified our neutralization assay to allow preincubation of the G4G7 or wild-type virions with our anti-NiV-G antisera, we still observed no differences in the IC_{50}s for the wild-type or G4G7 mutant virions (data not shown). We further observed that all entry-competent triple N-glycan mutant virions tested displayed levels of neutralization sensitivity similar to those of our single and most of our double N-glycan mutants (Fig. 4C). In summary, almost all virions tested displayed increased antibody neutralization sensitivity relative to wild-type virions, and no additional neutralization sensitivity was observed by removing multiple N-glycans simultaneously, compared to removing a single N-glycan. Overall, our data support a biological role for N-glycans in NiV-G in protecting NiV from antibody neutralization.

N-glycans modulate membrane fusion by multiple mechanisms. The mechanisms for the hyper- and hypofusogenic phenotypes of the NiV-G N-glycan mutants were explored by measuring receptor-induced conformational changes in NiV-G previously shown to affect NiV-F triggering (Fig. 5). We previously reported that ephrinB2 and ephrinB3 receptor binding to NiV-G induced a conformational change detectable by MAb45. Receptor-binding enhanced (RBE) the exposure of the MAb45 binding epitope in NiV-G at 37°C but not at 4°C, and the MAb45 RBE epitope exposure was shown to be important for F-triggering and membrane fusion (2). Using an identical receptor-free cell system, we measured the levels of receptor-induced exposure of the MAb45 epitope to our single (Fig. 5A), double (Fig. 5B), and triple (Fig. 5B) NiV-G N-glycan mutants. Importantly, all of the mutants that contained the G2 mutation (hypofusogenic in cell-cell fusion assays) did not result in any MAb45 binding enhancement, and some may have even resulted in a MAb45 binding decrease (particularly mutant G2G3G6) (Fig. 5A and B).

Interestingly, we observed the MAb45 RBE phenotype for hyperfusogenic mutant G6 above the levels of MAb45 binding enhancement observed for the wild-type NiV-G (Fig. 5A). These data suggest that the hyperfusogenic phenotype of mutant G6 may be explainable by its increased ability to induce a conformational change in G that triggers F, which is measurable by MAb45 bind-

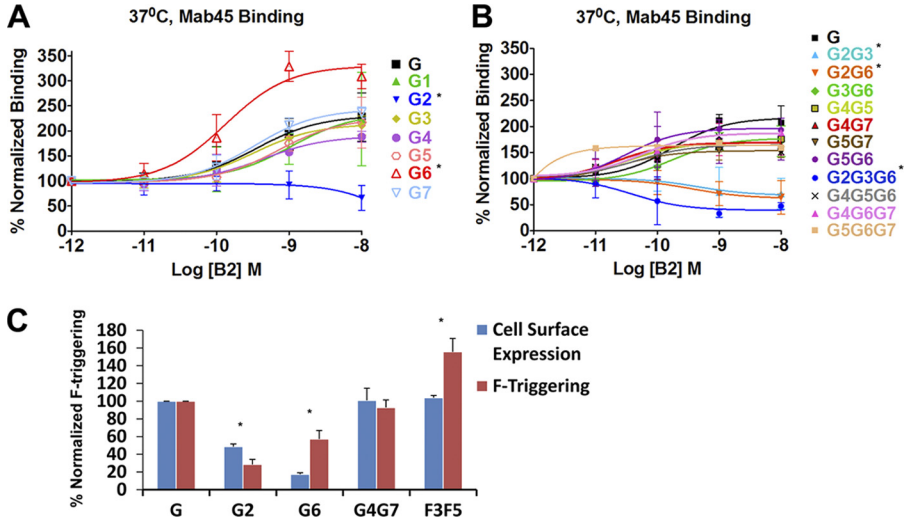

FIG 5 N-glycans modulate membrane fusion by distinct mechanisms. (A and B) Levels of binding of wild-type or single N-glycan mutant (A) or multiple N-glycan mutant (B) NiV-G glycoproteins to MAb45 at various concentrations of soluble ephrinB2 (B2). Binding of MAb45 to receptor-negative CHO cells expressing NiV-G was measured by flow cytometry. Binding signals were normalized to MAb45 binding in the absence of B2 (set at 100%). The data were plotted using Prism, and averages ± the standard deviations from four or more experiments are shown for the single (A) or double or triple (B) N-glycan mutants. *, Mutants for which *P* values calculated using Student *t* tests showed statistically significant differences ($P < 0.05$) between the wild-type and mutant levels of MAb45 binding over several log (B2) concentrations. (C) F triggering was measured by detecting the amount of binding of biotinylated NiV-F HR2 peptide to CHO cells coexpressing the NiV F and G glycoproteins, as performed by Aguilar et al. (2) and Aguilar et al. (1). For fair comparisons, the normalized cell surface expression levels of each NiV-G glycoprotein was plotted against normalized levels of F-triggering. The average of four independent experiments ± the standard deviation is shown. *, Mutants for which *P* values calculated using Student *t* tests showed statistically significant differences ($P < 0.05$) between the wild-type and mutant ratios of F triggering to CSE.

ing. In contrast, the hyperfusogenic mutant G4G7 displayed wild-type levels of MAb45 binding enhancement (Fig. 5B), even though it displayed 450% of the levels cell syncytium formation that the wild-type NiV-G induced (Fig. 2 and Table 1). These data indicate that the hyperfusogenic phenotype of mutant G4G7 is not due to an increase in the conformational change marked by MAb45 binding and must be due to a different step in the fusion cascade. Our data also indicate that the mechanisms that give rise to the hyperfusogenic phenotypes of mutants G6 and G4G7 are distinct.

To further explore the mechanisms by which our hyper- and hypofusogenic N-glycan mutants affect membrane fusion, we carried out a NiV-F triggering assay. This assay uses a NiV-F HR2-mimicking peptide that traps the F prehairpin intermediate conformation, a marker of NiV-F triggering. We have reported that this assay can measure relative levels of NiV-F triggering of distinct NiV-G or NiV-F fusion mutants (1, 2). We observed that while mutant G2 triggered lower than wild-type levels of NiV-F, mutant G6 triggered higher and G4G7 equal levels of NiV-F, respectively, when normalized to the mutant's levels of cell surface expression (Fig. 5C). Our positive control, the NiV-F mutant F3F5, was previously reported to be triggered at higher than wild-type NiV-F levels (1). Our data agree with the relative levels of receptor-induced MAb45 binding correlating with the F-triggering levels induced by mutants G6 and G4G7, further supporting the conclusion that these two NiV-G N-glycan mutants modulate membrane fusion by distinct mechanisms.

F/G interaction avidities and fusion phenotypes of the NiV-G N-glycan mutants. With the exception of human metapneumovirus (15, 41), the interactions between the paramyxovirus fusion and attachment glycoproteins have been shown to play crucial roles in membrane fusion (reviewed in references 17 and 18). Even for the paramyxovirus RSV, whose attachment protein is not absolutely required for membrane fusion, the presence of the attachment protein enhances fusion (20). We previously reported the detection of NiV-F and NiV-G interactions via a reciprocal coimmunoprecipitation assay (6, 24). We also reported a negative correlation between the avidity of F/G interactions and the fusogenic capacities of NiV-F N-glycan and cytoplasmic tail mutants, suggesting that dissociation of F and G may be important during NiV membrane fusion (5, 6). Thus, we set out to determine whether NiV F/G interaction avidities may account for some of the fusion phenotypes of our NiV-G N-glycan mutants.

Because it is widely accepted that the mature form of paramyxovirus F (F_1/F_2 complex) executes membrane fusion, we estimated the avidities of the interactions between NiV-F_1 and our NiV-G N-glycan mutants. We coimmunoprecipitated (co-IP) NiV-F_0 and NiV-F_1 from immunoprecipitates (IPs) obtained from viral lysates using anti-NiV-G specific antibodies (Fig. 6A). The relative strength of each band was quantified by measuring fluorescent antibody signals using a Li-Cor Odyssey instrument (see Materials and Methods). For accurate comparisons, the co-IP NiV-F signals (VL IP) were normalized to the total amounts of NiV-F_1 in viral lysates (VL) and to the levels of NiV-G immunoprecipitated from these viral lysates (VL IP) to account for any differences in the mutant's expression, viral glycoprotein incorporation, or immunoprecipitation (Fig. 6A). Thus, as previously performed (5, 6), to account for differences in expression of NiV-F in any given experiment, as well as to account for variations in the amounts of IP NiV-G per sample, we calculated a ratio between the levels of co-IP NiV-F and the corresponding amount of NiV-F in the total viral lysates and the amount of IP NiV-G per experiment and set this ratio (VL co-IP NiV-F)/(VL NiV-F)(VL IP

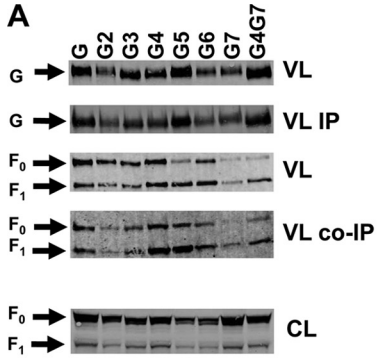

B

Env Protein	Fusion Index	Avidity of F_1/G Interactions	% F_1 in CL	% F_1 in VL	% F_1 in VL IP
G	1.0	1.0	18.3	30.2	48.9
G2	0.0	1.1	15.6	34.8	48.8
G3	0.9	1.3	20.3	40.2	45.9
G4	1.1	1.4	21.9	36.2	51.6
G5	0.7	2.5	12.6	54.2	67.7
G6	6.4	1.5	18.5	48.8	57.1
G7	1.6	1.3	16.5	56.0	60.4
G4G7	4.1	0.8	22.1	76.6	76.9

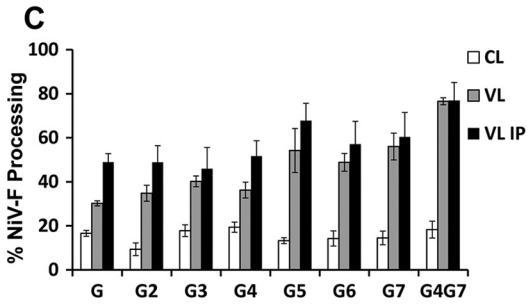

FIG 6 F/G interaction avidities do not account for fusion phenotypes. (A) Immunoprecipitation and coimmunoprecipitation of NiV-G and NiV-F, respectively, from 293T cell lysates. NiV/VSV-pseudotyped virions containing wild-type NiV-F and wild-type or mutant NiV-G were lysed and immunoprecipitated using protein G-magnetic beads conjugated to anti-HA antibodies. The immunoprecipitates containing directly immunoprecipitated (IP) and coimmunoprecipitated (co-IP) proteins were split in half and analyzed by Western blotting with anti-HA and anti-AU1 antibodies to detect G and F signals, respectively. The nonimmunoprecipitated viral lysates (VL) are also shown. (B) Table showing the fusion indexes, the relative avidities of NiV-F interactions with the wild-type or mutant NiV-G glycoproteins and the percentages of F_1 in cell lysates, viral lysates, and coimmunoprecipitated viral samples. To quantify the avidities of NiV F_1/G interactions, the signals in each F_1 or G band from panel A were quantified using a Li-Cor Imager and software. The avidity of F/G interactions is represented by the ratio of the amount of coimmunoprecipitated NiV-F_1 over the product of NiV-F_1 in the viral lysates and the immunoprecipitated NiV-G. Subsequently, all ratios were normalized to the ratio of the wild-type NiV-G set to 1, averaged from four independent experiments, and shown in comparison from the fusion indexes from Table 1. (C) The percentage of NiV-F cleavage was calculated as the percentage of F_1 in the total NiV-F (F_0 + F_1) in cell lysates, viral lysates, or immunoprecipitated viral samples. Averages ± the standard deviations from four experiments are shown.

NiV-G) for the wild-type to 1. Using this measurement, avidity values for a given mutant of less or more than 1.0 would indicate decreased or increased avidities of F/G interactions, respectively, relative to the avidity of the wild-type glycoproteins (5, 6). It is necessary to point out that the gel images shown in Fig. 6 correspond to one experiment only and do not necessarily visually reflect the avidity values calculated for every mutant in Fig. 1B, which are averages of four experiments.

In general, we observed that the fusion phenotypes of our NiV-G N-glycan mutants were not due to effects of N-glycan removal on F_1/G interaction avidities (Fig. 6A and B). Our results for the relative avidities of F_1/G interactions, averaged from three independent experiments, are shown in Fig. 6B. Except for mutant G5, all N-glycan mutants that affected fusion had near wild-type levels of F_1/G interaction avidities. Thus, our data indicate no correlation between fusion phenotypes and F/G interaction avidities for the NiV-G N-glycan mutants analyzed. Furthermore, our results indicate that the fusion phenotypes of our NiV-G N-glycan mutants are not due to their effects on the avidities of F_1/G interactions.

In addition, we noted that the NiV-F protein that was incorporated into G4G7 virions, and to a lesser extent G5 virions, appeared to be processed more efficiently than the F protein in wild-type virions (Fig. 6A). Quantification of the percentage of F_1 in the total sum of F_0 and F_1 in virions confirmed that the percentage of F_1 in viral lysates was higher (76.6%) than that in wild-type virions (30.2%). To determine whether the percentage of F_1 was due to an increase of F cleavage in cells that expressed G4G7, we calculated the percentage of F_1 in whole-cell lysates that expressed wild-type NiV-F and wild-type or mutant NiV-G. Our data indicated that NiV-F cleavage was not significantly enhanced in the presence of G4G7 in whole-cell lysates (22.1% of F_1 in the G4G7 cell lysates versus 18.3% F_1 in the wild-type G cell lysates). These data suggest that mutant G4G7 might enhance the incorporation of mature NiV F_1 into virions (Fig. 6B).

DISCUSSION

N-glycans on paramyxovirus glycoproteins have been reported to be required for proper protein expression, conformational integrity, and in some cases efficient membrane fusion (28, 36, 40, 44). However, our data revealed different functions for the NiV-G N-glycans. Evidently, some NiV-G N-glycans reduce fusion efficiency, since their removal caused cell-cell hyperfusogenicity and increased viral entry (Fig. 1 and 2). These data, in combination with our previous report that removal of N-glycans from NiV-F increases membrane fusion and viral entry, and similar data for HeV-F (9), strongly suggest that the roles of NiV N-glycans for the henipaviruses are unique compared to the roles of N-glycans for other paramyxovirus genera. Although the link between cell-cell fusion and viral entry is not well understood and there may be other yet unknown functions of the henipavirus N-glycans, our data also suggest that the henipaviral glycoproteins may have the capacity to mutate to induce greater levels of cell-cell fusion and viral entry than the currently known wild-type glycoproteins.

If most of the NiV-G N-glycans are not needed for proper glycoprotein expression, folding, and transport to the cell surface, what are their functions? Our data from the present study (Fig. 4) and from our previous report (6) indicate a role for the NiV-G and NiV-F N-glycans in shielding NiV against neutralizing antibodies. These results may impact henipavirus vaccine development, since

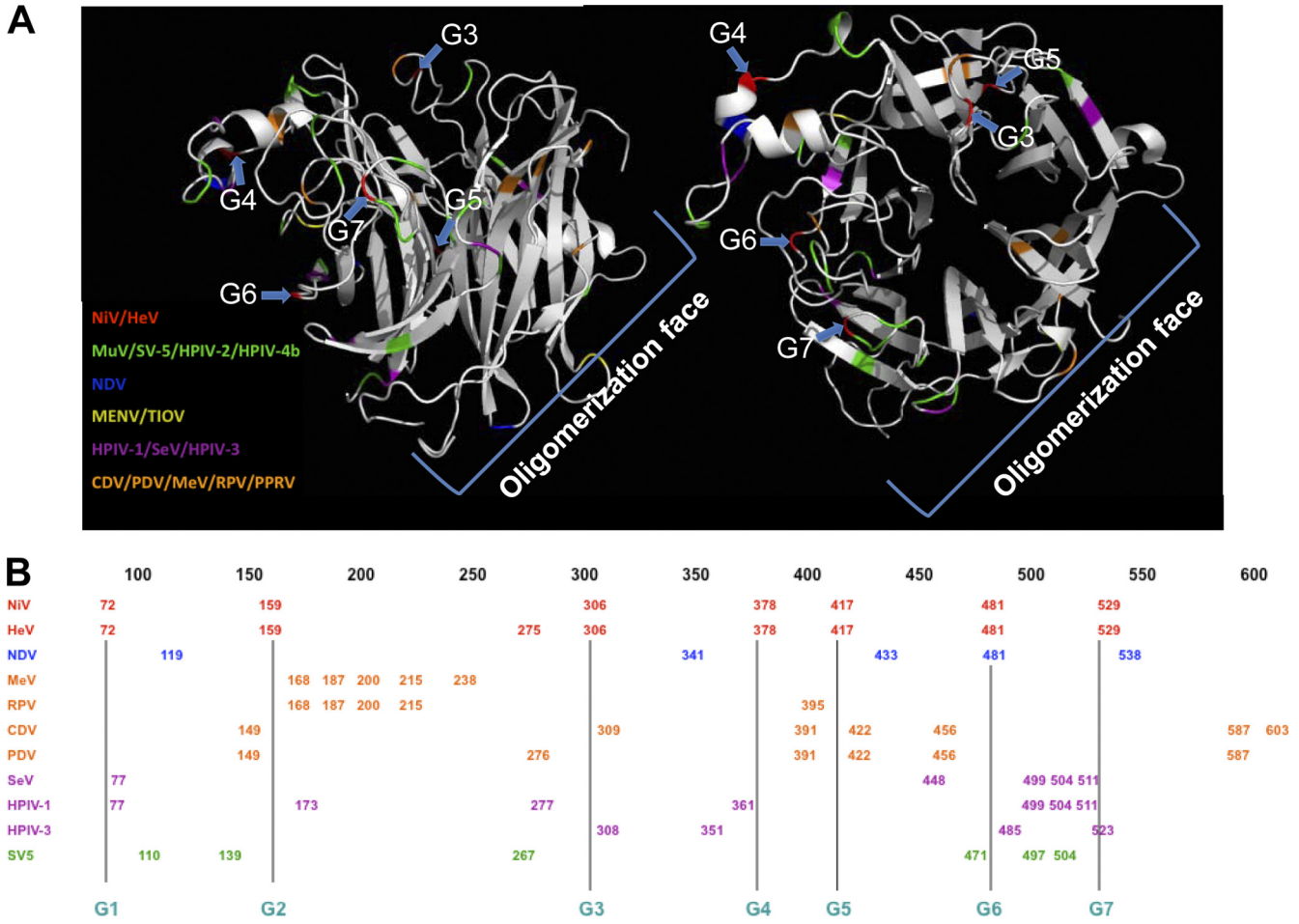

FIG 7 Comparison of N-glycan structural positions in the paramyxovirus genera. (A) Side-view (left) and top-view (right) ribbon representations of the monomer of NiV-G globular head domain, drawn using PYMOL (www.pymol.org) taken from Bowden et al. (7) (PDB code 2VSM). The structure displays the position of the NiV-G head N-glycosylation sites (G3-G7, shown in read and marked by blue arrows). The relative positions of N-glycosylation sites in other paramyxovirus attachment proteins (one representative virus for every genus) are highlighted: NiV (red, *Henipavirus*), SV-5 (simian parainfluenza virus 5, green, *Rubulavirus*), NDV (blue, *Avulavirus*), MENV (menangle virus, yellow, not classified), hPIV-1 (magenta, *Respirovirus*), and MeV (orange, *Morbillivirus*). The likely oligomerization face of NiV-G, according to the HeV-G dimeric structure from Bowden et al. (8a), is indicated. (B) The positions of the N-glycosylation sites for one to several members of each paramyxovirus genus are displayed in a linear scale. The colors for each genus are matched to those in the NiV-G structures in panel A.

increased neutralization sensitivity may result from increased glycoprotein peptide epitope exposure. Selective deglycosylation has been reported to result in broader and/or more potent neutralizing antibody responses for SIV, HBV, and EIAV (23, 38, 39). Thus, we speculate that some of our NiV-G N-glycan mutants may elicit improved neutralizing antibody responses. Again, although the roles of cell-cell fusion and viral entry during NiV disease are not completely understood, our data allow us to speculate that a coexisting function for the NiV and HeV N-glycans may be to suppress cell-cell fusion to allow the host to survive longer. This is an attractive possibility since syncytium formation is a hallmark of henipavirus pathobiology.

In our NiV-F N-glycan report, because of the physical location of the NiV-F N-glycans, we speculated that they might physically impede required conformational changes in NiV-F during membrane fusion, such as six-helix bundle formation (6). However, it remains to be determined whether the physical domains of the NiV-G N-glycans (Fig. 7) are directly involved in membrane fusion. In addition, we previously reported that N-glycans in NiV-F bind galectin-1, an innate immune system lectin, and this glycoprotein-lectin association suppresses cell-cell fusion (14, 24). Again, although the role of cell-cell fusion in the spread of NiV disease is not fully understood, these observations highlight alternative roles of henipavirus N-glycans, such as hijacking innate immunity lectins (such as galectin-1) to suppress cell-cell fusion levels to allow maximum host survival and viral spread. It remains to be determined whether the binding of henipavirus N-glycans to innate immunity lectins plays an important role in the establishment of a successful infection *in vivo*.

We observed synergistic and dominant-negative or antagonistic effects of N-glycans on membrane fusion and viral entry (Fig. 2 and 3). In addition, our results indicated that the functions of the NiV-G N-glycans in membrane fusion are highly context dependent. These context-dependent synergistic and antagonistic effects of N-glycan removal on membrane fusion indicate a high flexibility in the functions of N-glycans for the henipaviruses. To

our knowledge, such high flexibility in the function of N-glycans has not been previously reported for any other paramyxovirus.

Our results also showed that neither altered levels of cell surface expression, nor receptor binding, nor severe effects in F/G interactions, nor aberrant oligomerization was responsible for the membrane fusion phenotypes observed by NiV-G N-glycan removal (Fig. 1). These results indicate that some N-glycans in NiV-G, particularly G4, G6, and G7, truly modulate membrane fusion promotion and viral entry. Interestingly, the crystal structure of the head of NiV-G (side view Fig. 7A, left panel; top view Fig. 7A, right panel) displays all of the N-glycans on essentially one-half of the head (Fig. 7A, top-left in either view). Furthermore, the N-glycans whose removal had the strongest effects on membrane fusion and viral entry (G4, G6, and G7) appear to be clustered on a relatively small region of the surface of the head (Fig. 7A, left in either view) relative to the other (G3 and G5) N-glycans in the head (Fig. 7A, top right in either view). This distribution of N-glycans suggest that the G4/G6/G7 region plays an essential role in regulating membrane fusion for the henipaviruses. In addition, the distribution of N-glycans on one side of the head seems somewhat unique for henipaviruses, since N-glycans in the opposite side of the head (bottom right in both structures) can be seen for all other paramyxovirus genera (Fig. 7A). Thus, we speculate that the unique clustering of N-glycans on one side of the NiV-G head may influence the unique roles of N-glycans in membrane fusion and viral entry that we observed in the present study.

Here, we report at least three types of NiV-G fusion mutants distinct from those previously reported (Fig. 5). The G2 N-glycan mutant displayed no membrane fusion, low F-triggering, and no receptor-induced MAb45 epitope exposure enhancement, but, in contrast to our recently reported G stalk cysteine mutants (27), wild-type levels of oligomerization and no prereceptor binding enhancement of MAb45 epitope exposure. Our data for the G2 mutant suggest a link between oligomerization strength and overall prereceptor binding conformation of NiV-G. Because the G2 mutant is different from the cysteine mutants previously reported (since it is capable of wild-type levels of oligomerization and displays no prereceptor-induced MAb45 exposure but is still fusion dead and has low F-triggering capabilities), our G2 mutant data highlight the importance of the NiV-G stalk in F-triggering and MAb45 head epitope exposure. Our data also agree with a vertical transmission of a signal between the head and stalk of NiV-G that is important for F-triggering, as we previously proposed (2).

A different type of NiV-G fusion mutant was G6, which displayed enhanced levels of fusion, F-triggering, and MAb45 epitope exposure beyond the wild-type levels. Therefore, this mutant highlights the importance of the link between these three events. However, a distinct type of fusion mutant we found was G4G7, which displayed increased levels of fusion but no increase in F-triggering or receptor-induced MAb45 epitope exposure relative to the wild-type NiV-G. This mutant suggests that NiV-G may be involved in more than one step in the membrane fusion triggering cascade.

In addition, our results indicated that the avidities of F/G interactions do not account for the altered membrane fusion phenotypes of the NiV-G N-glycan mutants (Fig. 6). Furthermore, we previously reported that the fusogenic capabilities of the NiV-F N-glycan mutants inversely correlated with the avidities of F/G interactions (6). Moreover, NiV-F cytoplasmic tail mutants followed a similar pattern (5). These data supported the conclusion that NiV follows the "clamp" or "dissociation" model, also proposed for MeV, in which F/G or F/H dissociation is a rate-limiting step in membrane fusion (reviewed in references 4, 17, and 18). However, our NiV-G N-glycan mutants did not follow the same trend, since the avidity of F/G interactions for the NiV-G N-glycan mutants did not correlate to their fusogenic capabilities. Although the G/F_1 interactions may be key to the role of F in the F triggering and membrane fusion cascade, our results are consistent with the NiV-G/F_1 interactions not being the most critical parameter for the role of NiV-G in fusion promotion. Our data suggest that NiV-G may have roles in membrane fusion that extend beyond receptor binding and F triggering; for example, NiV-G may need to stay attached to the target membrane to ensure efficient fusion pore expansion. It will be interesting to explore this possibility or to determine whether NiV-G is able to modulate any other steps in the F conformational cascade that follow F triggering.

It remains to be determined whether the roles we observed for the NiV-G N-glycans are similar for the equivalent HeV-G N-glycans, especially since their positions in HeV-G are conserved, except for the addition of one potential N-glycosylation site in HeV-G at position N275 (Fig. 7B). The roles of N-glycans in NiV-F and HeV-F membrane fusion were found to be generally similar, although for unknown reasons, the membrane fusion phenotypes of NiV-F N-glycan mutants appeared generally stronger than the phenotypes of the HeV-F N-glycans at equivalent positions (6, 9, 31). Will similar roles be observed for equivalent N-glycans in NiV-G and HeV-G? Is the additional N-glycosylation site in HeV-G at position N275 N glycosylated and, if so, is it important for membrane fusion, viral entry, shielding against neutralizing antibodies, or other biological functions? Are similar N-glycans in HeV and NiV important for binding galectin-1 or other lectins in the innate immune system? The answers to these questions will likely enhance our understanding of the role of N-glycans on the pathobiology of these deadly emerging viruses. Furthermore, it remains to be determined whether some of the biological functions uncovered for the NiV and HeV F and G N-glycans are generalizable to other members of the paramyxovirus family whose N-glycans have not been yet studied.

ACKNOWLEDGMENTS

This study was supported by National Institutes of Health grants AI094329 to H.C.A. and AI069317 to B.L.

We sincerely thank Cristal Reyna for technical assistance and Anthony Nicola for critical reading of the manuscript.

REFERENCES

1. **Aguilar HC, Aspericueta V, Robinson LR, Aanensen KE, Lee B.** 2010. A quantitative and kinetic fusion protein-triggering assay can discern distinct steps in the Nipah virus membrane fusion cascade. J. Virol. **84**:8033–8041.
2. **Aguilar HC, et al.** 2009. A novel receptor-induced activation site in the Nipah virus attachment glycoprotein (G) involved in triggering the fusion glycoprotein (F). J. Biol. Chem. **284**:1628–1635.
3. **Aguilar HC, Iorio RM.** 2012. Henipavirus membrane fusion and viral entry. Curr. Top. Microbiol. Immunol. **359**:79–94.
4. **Aguilar HC, Lee B.** 2011. Emerging paramyxoviruses: molecular mechanisms and antiviral strategies. Expert Rev. Mol. Med. **13**:e6.
5. **Aguilar HC, et al.** 2007. Polybasic KKR motif in the cytoplasmic tail of Nipah virus fusion protein modulates membrane fusion by inside-out signaling. J. Virol. **81**:4520–4532.
6. **Aguilar HC, et al.** 2006. N-glycans on Nipah virus fusion protein protect

against neutralization but reduce membrane fusion and viral entry. J. Virol. **80**:4878–4889.
7. **Bowden TA, et al.** 2008. Structural basis of Nipah and Hendra virus attachment to their cell-surface receptor ephrin-B2. Nat. Struct. Mol. Biol. **15**:567–572.
8. **Bowden TA, et al.** 2008. Crystal structure and carbohydrate analysis of Nipah virus attachment glycoprotein: a template for antiviral and vaccine design. J. Virol. **82**:11628–11636.
8a. **Bowden TA, Crispin M, Harvey DJ, Jones EY, Stuart DI.** 2010. Dimeric architecture of the Hendra virus attachment glycoprotein: evidence for a conserved mode of assembly. J. Virol. **84**:6208–6217.
9. **Carter JR, Pager CT, Fowler SD, Dutch RE.** 2005. Role of N-linked glycosylation of the Hendra virus fusion protein. J. Virol. **79**:7922–7925.
10. **Cheng-Mayer C, Brown A, Harouse J, Luciw PA, Mayer AJ.** 1999. Selection for neutralization resistance of the simian/human immunodeficiency virus SHIVSF33A variant in vivo by virtue of sequence changes in the extracellular envelope glycoprotein that modify N-linked glycosylation. J. Virol. **73**:5294–5300.
11. **Chua KB, et al.** 2000. Nipah virus: a recently emergent deadly paramyxovirus. Science **288**:1432–1435.
12. **Colgrave ML, et al.** 2012. Site occupancy and glycan compositional analysis of two soluble recombinant forms of the attachment glycoprotein of Hendra virus. Glycobiology **22**:572–584.
13. **Davis D, Stephens DM, Willers C, Lachmann PJ.** 1990. Glycosylation governs the binding of antipeptide antibodies to regions of hypervariable amino acid sequence within recombinant gp120 of human immunodeficiency virus type 1. J. Gen. Virol. **71**(Pt 12):2889–2898.
14. **Garner OB, et al.** 2010. Endothelial galectin-1 binds to specific glycans on Nipah virus fusion protein and inhibits maturation, mobility, and function to block syncytia formation. PLoS Pathog. **6**:e1000993. doi:10.1371/journal.ppat.1000993.
15. **Herfst S, et al.** 2008. Low-pH-induced membrane fusion mediated by human metapneumovirus F protein is a rare, strain-dependent phenomenon. J. Virol. **82**:8891–8895.
16. **Iorio RM, Glickman RL, Sheehan JP.** 1992. Inhibition of fusion by neutralizing monoclonal antibodies to the haemagglutinin-neuraminidase glycoprotein of Newcastle disease virus. J. Gen. Virol. **73**(Pt 5):1167–1176.
17. **Iorio RM, Mahon PJ.** 2008. Paramyxoviruses: different receptors—different mechanisms of fusion. Trends Microbiol. **16**:135–137.
18. **Iorio RM, Melanson VR, Mahon PJ.** 2009. Glycoprotein interactions in paramyxovirus fusion. Future Virol. **4**:335–351.
19. **Johnson JB, Aguilar HC, Lee B, Parks GD.** 2011. Interactions of human complement with virus particles containing the Nipah virus glycoproteins. J. Virol. **85**:5940–5948.
20. **Kahn JS, Schnell MJ, Buonocore L, Rose JK.** 1999. Recombinant vesicular stomatitis virus expressing respiratory syncytial virus (RSV) glycoproteins: RSV fusion protein can mediate infection and cell fusion. Virology **254**:81–91.
21. **Lam SK.** 2003. Nipah virus-a potential agent of bioterrorism? Antivir. Res. **57**:113–119.
22. **Lamb RA, Paterson RG, Jardetzky TS.** 2006. Paramyxovirus membrane fusion: lessons from the F and HN atomic structures. Virology **344**:30–37.
23. **Lee J, Park JS, Moon JY, Kim KY, Moon HM.** 2003. The influence of glycosylation on secretion, stability, and immunogenicity of recombinant HBV pre-S antigen synthesized in *Saccharomyces cerevisiae*. Biochem. Biophys. Res. Commun. **303**:427–432.
24. **Levroney EL, et al.** 2005. Novel innate immune functions for galectin-1: galectin-1 inhibits cell fusion by Nipah virus envelope glycoproteins and augments dendritic cell secretion of proinflammatory cytokines. J. Immunol. **175**:413–420.
25. **Luby SP, et al.** 2009. Recurrent zoonotic transmission of Nipah virus into humans, Bangladesh, 2001–2007. Emerg. Infect. Dis. **15**:1229–1235.
26. **Luby SP, et al.** 2006. Foodborne transmission of Nipah virus, Bangladesh. Emerg. Infect. Dis. **12**:1888–1894.
27. **Maar D, et al.** 2012. Cysteines in the stalk of the nipah virus G glycoprotein are located in a distinct subdomain critical for fusion activation. J. Virol. **86**:6632–6642.
28. **McGinnes L, Sergel T, Reitter J, Morrison T.** 2001. Carbohydrate modifications of the NDV fusion protein heptad repeat domains influence maturation and fusion activity. Virology **283**:332–342.
29. **McGinnes LW, Morrison TG.** 1995. The role of individual oligosaccharide chains in the activities of the HN glycoprotein of Newcastle disease virus. Virology **212**:398–410.
30. **McKinnell JA, Saag MS.** 2009. Novel drug classes: entry inhibitors [enfuvirtide, chemokine (C-C motif) receptor 5 antagonists]. Curr. Opin. HIV AIDS **4**:513–517.
31. **Moll M, Kaufmann A, Maisner A.** 2004. Influence of N-glycans on processing and biological activity of the Nipah virus fusion protein. J. Virol. **78**:7274–7278.
32. **Murineddu G, Murruzzu C, Pinna GA.** 2010. An overview on different classes of viral entry and respiratory syncytial virus (RSV) fusion inhibitors. Curr. Med. Chem. **17**:1067–1091.
33. **Navarro-Sanchez E, et al.** 2003. Dendritic-cell-specific ICAM3-grabbing non-integrin is essential for the productive infection of human dendritic cells by mosquito-cell-derived dengue viruses. EMBO Rep. **4**:723–728.
34. **Negrete OA, et al.** 2005. EphrinB2 is the entry receptor for Nipah virus, an emergent deadly paramyxovirus. Nature **436**:401–405.
35. **Negrete OA, et al.** 2006. Two key residues in ephrinB3 are critical for its use as an alternative receptor for Nipah virus. PLoS Pathog. **2**:e7. doi:10.1371/journal.ppat.0020007.
36. **Olofsson S, Hansen JE.** 1998. Host cell glycosylation of viral glycoproteins: a battlefield for host defence and viral resistance. Scand. J. Infect. Dis. **30**:435–440.
37. **Pikora CA.** 2004. Glycosylation of the ENV spike of primate immunodeficiency viruses and antibody neutralization. Curr. HIV Res. **2**:243–254.
38. **Reitter JN, Means RE, Desrosiers RC.** 1998. A role for carbohydrates in immune evasion in AIDS. Nat. Med. **4**:679–684.
39. **Salinovich O, et al.** 1986. Rapid emergence of novel antigenic and genetic variants of equine infectious anemia virus during persistent infection. J. Virol. **57**:71–80.
40. **Sawatsky B, von Messling V.** 2010. Canine distemper viruses expressing a hemagglutinin without N-glycans lose virulence but retain immunosuppression. J. Virol. **84**:2753–2761.
41. **Schowalter RM, Smith SE, Dutch RE.** 2006. Characterization of human metapneumovirus F protein-promoted membrane fusion: critical roles for proteolytic processing and low pH. J. Virol. **80**:10931–10941.
42. **Skehel JJ, et al.** 1984. A carbohydrate side chain on hemagglutinins of Hong Kong influenza viruses inhibits recognition by a monoclonal antibody. Proc. Natl. Acad. Sci. U. S. A. **81**:1779–1783.
43. **Tan CT, Wong KT.** 2003. Nipah encephalitis outbreak in Malaysia. Ann. Acad. Med. Singapore **32**:112–117.
44. **von Messling V, Cattaneo R.** 2003. N-linked glycans with similar location in the fusion protein head modulate paramyxovirus fusion. J. Virol. **77**:10202–10212.
45. **Wei X, et al.** 2003. Antibody neutralization and escape by HIV-1. Nature **422**:307–312.
46. **Whitman SD, Smith EC, Dutch RE.** 2009. Differential rates of protein folding and cellular trafficking for the Hendra virus F and G proteins: implications for F-G complex formation. J. Virol. **83**:8998–9001.
47. **Wong KT, et al.** 2002. Nipah virus infection: pathology and pathogenesis of an emerging paramyxoviral zoonosis. Am. J. Pathol. **161**:2153–2167.
48. **Xu K, et al.** 2008. Host cell recognition by the henipaviruses: crystal structures of the Nipah G attachment glycoprotein and its complex with ephrin-B3. Proc. Natl. Acad. Sci. U. S. A. **105**:9953–9958.
49. **Xu Y, et al.** 2004. Crystallization and preliminary crystallographic analysis of the fusion core from two new zoonotic paramyxoviruses, Nipah virus and Hendra virus. Acta Crystallogr. D Biol. Crystallogr. **60**:1161–1164.